

Low Noise, High-Speed InP/InGaAs HBTs

Shawn S.H. Hsu, Dimitris Pavlidis

Department of Electrical Engineering and Computer Science,
The University of Michigan, Ann Arbor, MI 48109-2122, USA

Tel: (734) 647-1778, Fax: (734) 763-6132, email: pavlidis@umich.edu, http://www.eecs.umich.edu/dp-group

Minoru Ida, and Takatomo Enoki

NTT Photonics Laboratories, NTT Corporation, 3-1, Morinosato Wakamiya,
Atsugi-shi, Kanagawa Pref. Japan 243-0198

Abstract

High frequency noise characteristics of InP/InGaAs HBTs with various emitter geometries were investigated. A minimum noise figure (F_{min}) of 1.51 dB and associated gain (G_a) of 9.6 dB at a frequency of 10 GHz and a DC power consumption of only 1.6 mW ($V_{CE}=1.6$ V, $I_C=1$ mA) at 10 GHz were obtained. The dependence of noise characteristics on bias and geometry is also reported. The dominant noise sources in these HBTs were analyzed and an optimum emitter area of $1.2 \times 20 \mu\text{m}^2$ was found to present minimum noise figure and equivalent noise resistance.

I. Introduction

The demand on high-speed transistors and circuits with low-noise figure and low-power consumption increased dramatically over the past few years due to the exponential growth of wireless and fiber communication market. InP-based HBTs attract a great interest due to their high-speed and high power density related to the inherent properties of the materials used and the vertical design approach of the devices. The high-frequency noise characteristics of HBTs have been previously reported [1-3]. However, only few reports addressed the noise characteristics of HBTs using InP-based materials, which have not been studied in detail. In this study, the noise performance of InP/InGaAs HBTs with various geometries was evaluated under different bias conditions at microwave frequencies (X-band). Equivalent circuit models that include device noise sources were also extracted. In addition, the dominant noise sources were analyzed and discussed. The results obtained demonstrate that InP-based HBTs exhibit excellent high frequency noise and gain characteristics under low power consumption, which are suitable candidates for high-frequency low-noise circuit applications.

II. Devices Structure and Microwave Characteristics

The InP-based HBTs were grown using MOCVD. The emitter layer is 30-nm-thick InP, the base is 50-nm-thick InGaAs carbon-doped to $3.7 \times 10^{19} \text{cm}^{-3}$ and the collector is 300-nm-thick InGaAs. Due to the reduced device size and high mobility of InP-based materials, the devices exhibit impressive maximum oscillation frequency (f_{max}) and cutoff frequency (f_T) characteristics. Table I summarizes f_T and f_{max} and the corresponding bias points of typical devices used in this study. For submicrometer emitter size devices, the f_{max} can reach 200 GHz at very low DC power level (~ 10 mW). Note that f_T increases as the emitter length varies from $20 \mu\text{m}$ to $5 \mu\text{m}$. This is mainly due to the reduced junction capacitances. However, as the emitter width reduces (from $1.2 \mu\text{m}$ to $0.6 \mu\text{m}$), the values of f_T do not increase correspondingly. The increased emitter resistance and lowered current level lead to an increased RC time constant and may be responsible for the reduced f_T of submicrometer devices.

| Device size (μm^2) | f_T (GHz) | f_{max} (GHz) | I_C (mA) | V_{CE} (V) |
|---------------------------------|-------------|-----------------|------------|--------------|
| 0.6x5 | 123 | 202 | 6.26 | 1.6 |
| 0.8x5 | 120 | 200 | 6.96 | 1.6 |
| 1.2x5 | 134 | 168 | 8.35 | 1.6 |
| 1.2x10 | 128 | 141 | 10.13 | 1.6 |
| 1.2x20 | 110 | 123 | 12.20 | 1.6 |

Table I: f_{max} , f_T and bias conditions for InP- HBTs with various emitter sizes

III. High Frequency Noise Characteristics

Noise measurements were performed from 6 to 14 GHz using an in-house developed automatic noise figure measurement setup with a FOCUS electromechanical tuner. The tests provided information on noise parameters

including the minimum noise figure (F_{min}), minimum source reflection coefficient (Γ_{min}), associated gain (G_a) and the equivalent noise resistance (R_n). In order to understand the dominant noise sources of these devices, the impact of various parameters such as bias condition (V_{CE} and I_C), emitter width and length on device noise performance was investigated.

a. Bias dependence

The impact of bias conditions on device F_{min} was first examined. The device tested had a $1.2 \times 10 \mu\text{m}^2$ emitter with 2-fingers and was biased at $V_{CE} = 1.6$ V. The noise figure was measured for collector currents varying from 0.5 mA to 7 mA. F_{min} varied by 0.41 dB from a minimum value of 1.97 dB at $I_C = 1$ mA to a maximum value of 2.38 dB at $I_C = 7$ mA, while G_a varied from 4.1 dB to 17.9 dB. The results suggest that shot noise contributed from collector current is not the dominant noise source since F_{min} varied only slightly for a considerable change of the associated gain. The results also indicate that the base and emitter parasitic resistance dominate the noise characteristics over a small bias current range while base current shot noise becomes obvious as the total current increases. The HBT was also measured under different collector voltages while keeping the collector current at 2 mA. The results show that F_{min} is kept almost constant over a wide range of collector voltage values. Fig.1 shows the measured results. One can see that InP-based HBTs present low noise characteristics over a wide range of bias conditions, which is an

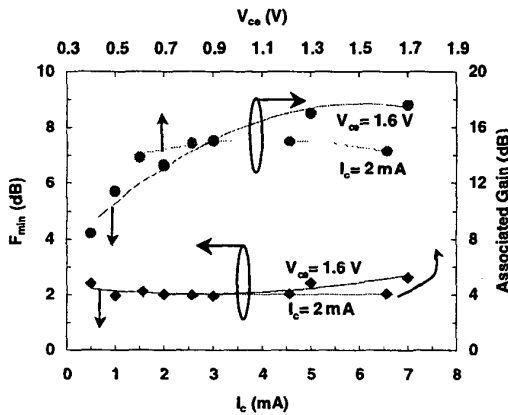


Fig. 1: F_{min} and G_a characteristics for a $1.2 \times 10 \mu\text{m}^2$, 2-finger InP/InGaAs HBT

attractive feature for low-noise circuit applications.

b. Emitter length dependence

Devices with the same emitter width ($1.2 \mu\text{m}$) and different lengths ($5 \mu\text{m}$, $10 \mu\text{m}$ and $20 \mu\text{m}$) were also investigated. The noise performance of devices biased under $V_{CE} = 1.6$ V at 10 GHz is shown in Fig. 2. The minimum noise figure increased as the emitter length decreased. As can be seen, devices with higher gain present higher noise figure. Since under the same collector current, the input-referred noise contributed from collector shot noise will be reversed proportional to the value of gain square, this implies that the collector current shot noise is not important. The results support the fact that input parasitic resistance thermal noise and base current shot noise dominate the noise characteristics in the evaluated InP-based HBTs.

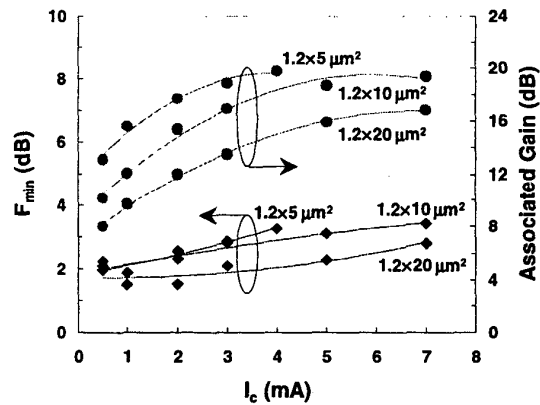


Fig. 2: F_{min} and G_a characteristics for InP/InGaAs HBTs with different emitter lengths

c. Emitter width dependence

Devices with the same emitter length but different widths were also tested. Three devices with emitter widths of $0.6 \mu\text{m}$, $0.8 \mu\text{m}$ and $1.2 \mu\text{m}$ and a emitter length of $5 \mu\text{m}$ were characterized and the results are shown in Fig. 3. The results indicate that devices with shorter emitter width have higher F_{min} . The dependence of noise characteristics on device geometry is analyzed by use of device small-signal model parameters as explained in Section IV.

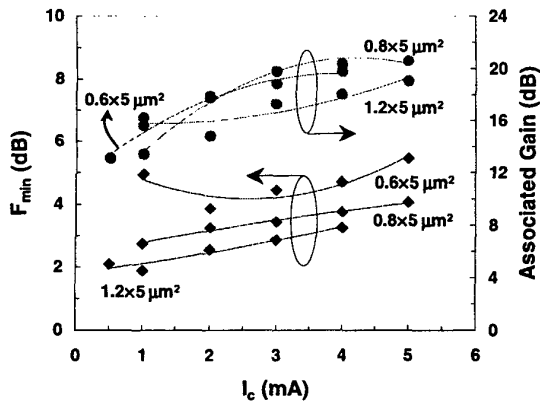


Fig. 3: F_{min} and G_a characteristics for InP/InGaAs HBTs with different emitter widths

d. Frequency dependence

Noise characteristics of these devices were also investigated as a function of frequency. F_{min} varied from 1.6 dB to 2.32 dB for the $1.2 \times 20 \mu\text{m}^2$ device and 2.1 dB to 2.52 dB for the $2.0 \times 10 \mu\text{m}^2$ device in the frequency range of 6 to 14 GHz. The respective change of G_a was from 17.4 dB to 9.8 dB and 17.0 dB to 10.1 dB. Although G_a varied, F_{min} maintained a relatively stable value over the entire measured range, which indicates that the InP HBTs of this study demonstrate good noise figure over a wide frequency range.

IV. Small-signal and Noise Equivalent Circuit Model

In order to further investigate the noise characteristics of the InP/InGaAs devices quantitatively, an HBT equivalent circuit small-signal model (T-model) was used. Fig. 4 shows the equivalent circuit model including noise sources. Note that the base and collector resistance, and B-C junction capacitance are separated into internal and external elements for a better physical representation of the device model. In addition, two correlated current noise sources and five voltage sources are employed to model the shot noise originating from two device junctions and the thermal noise related to parasitic resistances, respectively.

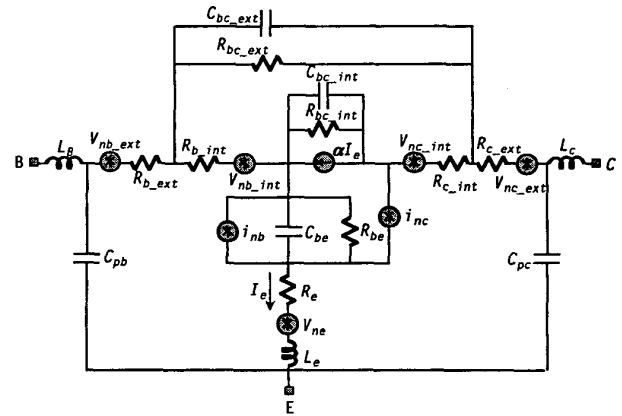


Fig. 4: Small-signal HBT model including noise sources

Small-signal model parameters were extracted directly from measured S -parameters under both “cold” and “hot” bias conditions [4]. Extraction was performed on multiple bias points simultaneously to improve convergence and obtain more accurate parameters. The measured and simulated S -parameters for a $1.2 \times 20 \mu\text{m}^2$ HBT are shown in Fig. 5 from 0.5 to 25.5 GHz at $I_C = 4.9 \text{ mA}$ and $V_{CE} = 1.6 \text{ V}$. Once the model parameters for the noiseless circuit are determined, the thermal noise and shot noise sources can be calculated [5]. Fig. 6 shows the result of measured and simulated F_{min} and G_a for a $1.2 \times 20 \mu\text{m}^2$ HBT under $I_C = 2.0 \text{ mA}$ and $V_{CE} = 1.6 \text{ V}$ from 6 to 14 GHz. As can be seen, excellent agreement between measured and simulated results is obtained for the S -parameters, as well as, F_{min} and G_a .

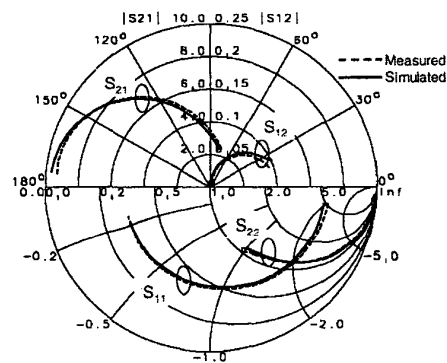


Fig. 5: Measured and simulated S -parameters for the $1.2 \times 20 \mu\text{m}^2$ HBT ($I_C = 4.9 \text{ mA}$, $V_{CE} = 1.6 \text{ V}$)

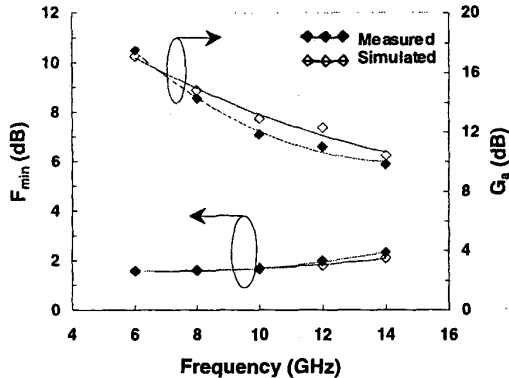


Fig. 6: Measured and simulated F_{min} and G_a for the $1.2 \times 20 \mu\text{m}^2$ HBT ($I_C = 2.0 \text{ mA}$, $V_{CE} = 1.6 \text{ V}$)

From the extracted equivalent circuit model parameters, the device noise characteristics can be analyzed quantitatively. C_d (B-E junction depletion capacitance at $V_{BE} = 0 \text{ V}$) and C_{BC} (B-C junction depletion capacitance at $V_{BC} = 0 \text{ V}$) were both scaled down with emitter area. Capacitance values as small as $\sim 10 \text{ fF}$ for both C_{BC} and C_d were obtained for sub-micron devices. In addition, the base and emitter resistances are found to contribute to a major portion to device input-referred noise. By comparing devices with the same emitter length ($5 \mu\text{m}$), one can see that even though the base resistance decreases with emitter width, the emitter resistance increases. The net result of these variations leads in an increase of F_{min} . Similarly, for devices with the same emitter width ($1.2 \mu\text{m}$), F_{min} increases as the emitter length reduces since both base and emitter resistances increase as well.

V. Discussion

Table II summarizes the F_{min} , G_a , R_n and bias currents of the devices at 10 GHz. As can be seen, the $1.2 \times 20 \mu\text{m}^2$ device is an optimum geometry, which shows best minimum noise figure and smallest equivalent noise resistance. In addition, the collector bias for best noise performance is only around 1 mA. The comparison of devices with different geometries suggests that smaller devices show higher noise figure and equivalent noise resistance. This appears to be related to their higher parasitic resistance. Moreover, devices with higher gain do not necessarily present smaller noise figure. Overall, it appears that the noise sources existing at the input of the devices and dominating the

noise performance are the base and emitter resistances (thermal noise) and base current (shot noise). As can be seen, the $0.6 \times 5 \mu\text{m}^2$ HBT shows the highest F_{min} due to its smaller geometry and higher base current.

| Device size (μm^2) | F_{min} (dB) | G_a (dB) | R_n (Ω) | I_C (mA) | I_B (μA) |
|---------------------------------|----------------|------------|--------------------|------------|-------------------------|
| 0.6×5 | 3.86 | 13.8 | 141.3 | 2.0 | 91 |
| 0.8×5 | 2.74 | 13.41 | 200 | 1.0 | 43 |
| 1.2×5 | 1.88 | 15.6 | 89.4 | 1.0 | 37 |
| 1.2×10 | 1.87 | 12.04 | 66.3 | 1.0 | 33 |
| 1.2×20 | 1.53 | 11.9 | 49 | 1.0 | 32 |

Table II: Device noise parameters and bias conditions

VI. Conclusions

In summary, the high-frequency noise characteristics of InP-based HBTs have been investigated and the optimum device geometry and bias condition was evaluated. The dominant noise sources were also analyzed. The results demonstrate that InP-based HBTs present high f_T and f_{max} at low operating current and voltage, which are very promising for low-noise, high-speed applications.

Acknowledgement: Work supported by ARO (MURI Contract No. DAAHO4-96-1-0001) and NTT.

[References]

- [1] G. N. Henderson, and D.W. Wu, "Noise characteristics of GaAs HBT's," *IEEE MTT-S International Microwave Symposium Digest*, v 3 1996, Piscataway, NJ, pp. 1221-1224
- [2] H. Schumacher, U. Erben, and W. Duerr, "SiGe heterojunction bipolar transistors - the noise perspective," *Journal of Solid-state electronics*, vol. 41, no. 10, pp. 1485-1492, Oct. 1997
- [3] M. T. Fresina, D. A. Ahmari, P.J. Mares, Q.J. Hartmann, M. Feng, and G.E. Stillman, "High-speed, low-noise InGaP/GaAs heterojunction bipolar transistors," *IEEE Electron Device Letters*, v 16, n 12, pp. 540-541, Dec. 1995
- [4] D.R. Pehlke and D. Pavlidis, "Evaluation of the factors determining HBT high-frequency performance by direct analysis of S -parameter data," *IEEE Trans. Microwave Theory Tech.*, vol. 40, no. 12, pp. 2367-2373, Dec. 1992
- [5] R. J. Hawkins, "Limitations of Nielsen's and related noise equations applied to microwave bipolar transistors, and a new expression for the frequency and current dependent noise figure," *Solid-State electronics*, vol.20, pp. 191-196, 1977